

# Transdermal Administration of Nanobody Molecules using Hydrogel-Forming Microarray Patch Technology: A Unique Delivery Approach

Aaron R. J. Hutton, Melissa Kirkby, Tom Van Bogaert, Peter Casteels, Christelle Nonne, Veronique De Brabandere, Ortwin Van de Vyver, Lalit K. Vora, Ismaiel A. Tekko, Helen O. McCarthy, and Ryan F. Donnelly\*

Nanobody molecules, derived from heavy-chain only antibodies in camelids, represent the next generation of biotherapeutics. In addition to low immunogenicity, high stability, and potency, their single-domain format facilitates the construction of multivalent molecules for therapeutic applications. Although predominantly administered using a hypodermic syringe and needle, alternative delivery methods are under investigation. That said, the transdermal route has yet to be explored. Therefore, microarray patch (MAP) technology, offering a potentially high dose, pain-free transdermal system, is employed in this study. Trivalent Nanobody molecules, with and without half-life extension (VHH and VHH[HLE]), are formulated into hydrogel-forming MAPs, with pharmacokinetic parameters assessed in Sprague–Dawley rats. VHH MAPs exhibited a sustained release profile, with a serum concentration of  $19 \pm 9 \text{ ng mL}^{-1}$  24 h post-administration. In contrast, a subcutaneous (SC) injection showed faster clearance, with a serum concentration of  $1.1 \pm 0.4 \text{ ng mL}^{-1}$  at 24 h. For VHH(HLE), both SC and MAP cohorts achieved a maximum serum concentration ( $T_{\text{max}}$ ) at 24 h. The MAP cohort displayed a notable increase in VHH(HLE) serum levels between 6–24 h, dropping after MAP removal. This study has exemplified MAPs potential for delivering advanced biologics, indicating the transdermal route's promise for pain-free, patient-friendly administration of Nanobody molecules.

## 1. Introduction

It is well established that all camelids have unique antibody-like structures that play a key role in the host immune response. In contrast to the well-conserved structure of immunoglobulin G (IgG) in mammals, which consists of two heavy chains and two light chains, camelids possess an additional IgG isotype composed of a homodimer of heavy chains only.<sup>[1,2]</sup> The lack of a light chain therefore reduces the antigen-binding fragment to a single variable domain, termed VHH (which is the basis for Nanobody molecules). Owing to this simplified, single-domain format the construction of multivalent molecules for therapeutic applications is less expensive than that for monoclonal antibodies (mAbs). One such therapeutic Nanobody molecule, caplacizumab, is a bivalent domain that has been designed to target the ultra-large von Willebrand factor, a glycoprotein that plays a key role in acquired thrombotic thrombocytopenic purpura (aTTP), a rare blood disorder in which platelet aggregation leads to microvascular thrombosis.<sup>[3]</sup> This treatment strategy has had a positive impact on TTP patients, with those on caplacizumab 1.55 times more likely to achieve a recovery of their platelet counts

A. R. J. Hutton, M. Kirkby, L. K. Vora, I. A. Tekko, H. O. McCarthy, R. F. Donnelly  
School of Pharmacy  
Queen's University Belfast  
97 Lisburn Road, Belfast BT9 7BL, Northern Ireland  
E-mail: [r.donnelly@qub.ac.uk](mailto:r.donnelly@qub.ac.uk)

T. Van Bogaert, P. Casteels, C. Nonne, V. De Brabandere, O. V. de Vyver  
R&D  
Sanofi Ghent  
Technologiepark 21, Zwijnaarde 9052, Belgium  
I. A. Tekko  
R&D  
Norbrook Laboratories Ltd  
Newry BT35 6QQ, Northern Ireland

 The ORCID identification number(s) for the author(s) of this article can be found under <https://doi.org/10.1002/mame.202400029>

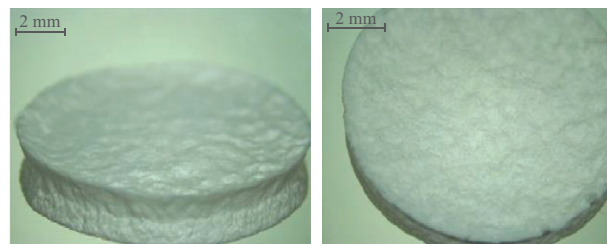
© 2024 The Authors. Macromolecular Materials and Engineering published by Wiley-VCH GmbH. This is an open access article under the terms of the [Creative Commons Attribution](https://creativecommons.org/licenses/by/4.0/) License, which permits use, distribution and reproduction in any medium, provided the original work is properly cited.

DOI: [10.1002/mame.202400029](https://doi.org/10.1002/mame.202400029)

when compared to standard plasma exchange therapy.<sup>[4]</sup> This is one example of the therapeutic potential of this next generation of biologics.

Nanobody molecules are also intrinsically stable molecules that can bind to conformational epitopes that may be otherwise inaccessible to mAbs due to their extended complimentary-determining region (CDR3) loops.<sup>[5]</sup> The enhanced stability has enabled Nanobody molecules to withstand different administration routes. For instance, ALX-0171, a homotrivalent construct that specifically targets human respiratory syncytial virus (hRSV) has been successfully administered via inhalation. Nanobody molecules have also been investigated for the treatment of mucosal infectious diseases caused by enterotoxigenic *Escherichia coli* (ETEC).<sup>[6]</sup> This is estimated to cause  $\approx 380\,000$  deaths annually during sporadic or epidemic outbreaks worldwide. Oral administration of Nanobody molecules led to a significant reduction of bacterial colonization in a mouse model. Moreover, Nanobody molecules extended the inhibitory activity in mouse colonization compared to commercial hyperimmune bovine colostrum products used for the prevention of ETEC-induced diarrhea.

Currently, the delivery of Nanobody molecules via the transdermal route has yet to be investigated. Clearly, these novel biomolecules do not possess the required properties for passive diffusion through the stratum corneum. Therefore, a traditional transdermal patch could not deliver therapeutic doses of Nanobody molecules to the systemic circulation. To this end, microarray patch (MAP) technology is a credible option to overcome the stratum corneum to deliver Nanobody molecules directly to the dermis and subcutaneous layers. This would have a number of advantages over the intravenous (IV) or subcutaneous (SC) route, such as pain-free administration, increased patient acceptance, prevention of needle stick injury, and elimination of sharps disposal. Furthermore, previous work has shown that repeat application of hydrogel-forming MAPs does not lead to prolonged skin reactions or prolonged disruption of skin barrier function.<sup>[7]</sup> Therefore, this work investigates the feasibility of delivering two trivalent model Nanobody molecules transdermally using two separate hydrogel-forming MAP systems by directly comparing the pharmacokinetic profile of this delivery system in Sprague–Dawley rats with an SC injection, currently the preferred method of administration. More specifically, a Nanobody molecule (named VHH) with a molecular weight (MW) of 45 kDa will be incorporated into a hydrogel-forming MAP system. This is a trivalent construct composed of three VHH domains that have no endogenous target in rat models thus enabling the general pharmacokinetic (PK) behavior of the Nanobody molecule to be assessed. The second Nanobody molecule (named VHH(HLE)) has been designed to improve the PK properties, that is, extension of half-life in systemic circulation by binding to rat serum albumin. Again, this is a trivalent construct with a MW of 45 kDa, composed of two VHH domains that do not bind to any rat target and one anti-albumin VHH domain. Binding to albumin as a carrier has been shown to lead to retention of the bound protein in circulation, with a resident time  $\approx 376$ -fold higher than its VHH counterpart in cynomolgus monkeys.<sup>[8]</sup> Therefore, formulation and delivery of both VHH and VHH(HLE) from a hydrogel-forming MAP will provide insights into manufacturing develop-



**Figure 1.** VHH(HLE) loaded lyophilized wafer (H1) composed of 5.6% w/w gelatin, 20% w/w mannitol, 5.6% w/w NaCl, and 3% w/w HLE-IRR VHH.

ment and the therapeutic potential of a unique transdermal delivery system for Nanobody molecules.

## 2. Results

### 2.1. Fabrication of VHH- and VHH(HLE)-Loaded Lyophilized Wafers

Eight different VHH formulations were prepared using an iterative approach as displayed in Table 1. F1–F5 were extremely brittle, resulting in all five formulations possessing poor structural integrity. Increasing the gelatin content as shown with F6 improved the structural integrity, however, increasing wafer size permitted a higher drug loading, as depicted with F7 and F8. Both F7 and F8 remained intact but the outer surface of F7 had collapsed superficially. Increasing the gelatin content, as shown with F8, produced a homogeneous wafer with good structural integrity. Using the same composition as wafer F8, VHH(HLE) loaded lyophilized wafers (H1) were homogeneous and remained structurally intact during demolding (Figure 1).


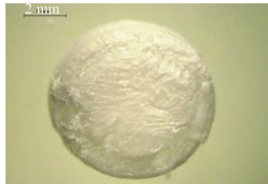

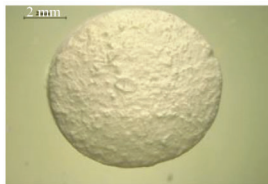

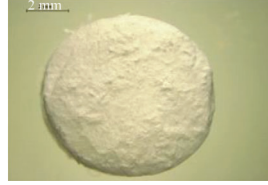

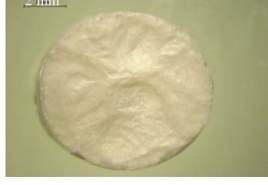

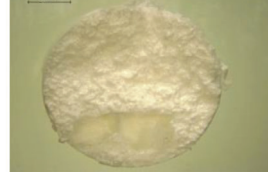





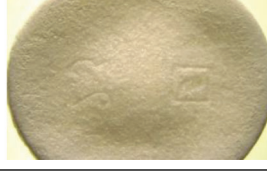
### 2.2. Strength Testing of VHH- and VHH(HLE)-Loaded Lyophilized Wafers

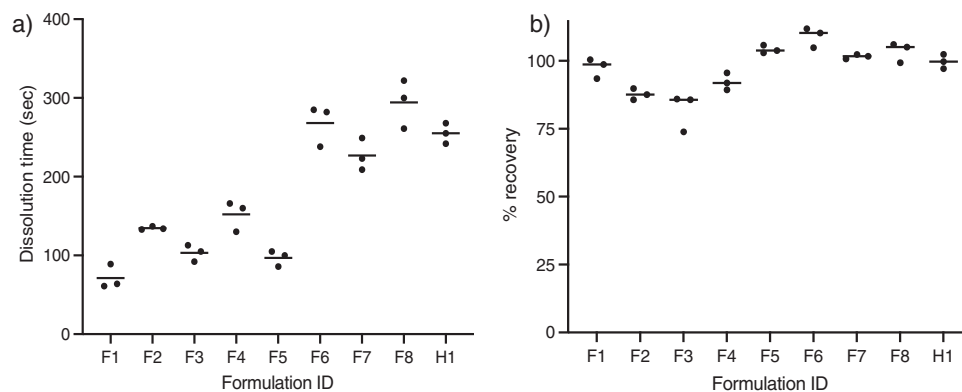
In a clinical setting, it is assumed that for practicality purposes, a hydrogel-forming MAP and its associated wafer will be applied in a single step. Therefore, it was of interest to determine the strength of the wafers, to ensure that upon MAP insertion into the skin, the wafer remained intact. F1–F5 crumbled during the application of 30 N force, thus failing this test as shown in Table 1. F6, F7, F8, and H1 remained structurally intact after compression of 30 N, showing that these wafers displayed the required mechanical strength for skin application.

### 2.3. Dissolution Time and Recovery of VHH- and VHH(HLE)-Loaded Lyophilized Wafers

Upon visual inspection, each formulation underwent complete dissolution in less than 5 min. F1 had the fastest dissolution time (70 s), however, as it displayed poor structural integrity, it was not considered suitable for in vitro experiments (Figure 2a). As expected, increasing the gelatin content prolonged the dissolution

**Table 1.** F1–F8 lyophilized wafers produced using different combinations of gelatin, mannitol, NaCl, and VHH.

| Formulation ID | Gelatin [% w/w] | Mannitol [% w/w] | NaCl [%w/w] | VHH [mg] | Result of 30 N compression test (pass/fail) | Structural morphology  |   |
|----------------|-----------------|------------------|-------------|----------|---|--|---|
| F1             | 1.1             | –                | 5.6         | 8.5      | Fail  |    |    |
| F2             | 1.1             | 5.6              | 5.6         | 8.5      | Fail  |    |    |
| F3             | 1.1             | 11.2             | 5.6         | 8.5      | Fail  |    |    |
| F4             | 2.8             | 11.2             | 5.6         | 8.5      | Fail  |   |   |
| F5             | 2.8             | 16.8             | 5.6         | 8.5      | Fail  |  |  |
| F6             | 5.6             | 16.8             | 5.6         | 8.5      | Pass  |  |  |
| F7             | 2.8             | 20               | 5.6         | 15       | Pass  |  |  |
| F8             | 5.6             | 20               | 5.6         | 15       | Pass  |  |  |



**Figure 2.** a) Dissolution times for F1–F8 and H1 lyophilized wafers in PBS (pH 7.4) at 37 °C and stirred at 200 rpm. Means + SD.,  $n = 3$ . b) Percentage drug recovery from F1–F8 and H1 lyophilized wafers following complete dissolution in PBS (pH 7.4) maintained at 37 °C and stirred at 200 rpm. Means + SD.,  $n = 3$ .

time with F8 dissolving at a significantly slower rate than F1 ( $p < 0.05$ ). All other pairwise comparisons indicated no significant difference in dissolution time. Despite this, there must be a trade-off between a short dissolution time, typically  $< 10$  min, and suitable structural integrity. F8 had the slowest dissolution time (288 s), yet this formulation produced a structurally intact wafer. Furthermore, H1 had a dissolution time of  $255 \pm 13$  s, which was deemed to be statistically insignificant when compared to F8 ( $p = 0.200$ ).

VHH and VHH(HLE) recovery was determined using SE-HPLC as detailed above. Drug recovery was determined by comparing the theoretical loading with the API recovered following dissolution. Therefore, due to the manual filling of the formulation into the molds, variability was to be expected. Nevertheless, comparing F1–F8, F3 had the lowest recovery ( $82 \pm 7\%$ ), with F6 yielding the greatest drug recovery ( $109 \pm 4\%$ ) (Figure 2b). As mentioned previously, there must be a trade-off between dissolution time and structural integrity, as well as with VHH recovery. F8, a homogeneous, intact wafer with suitable mechanical strength had a drug recovery of  $103 \pm 4\%$ . For this reason, F8 was considered the most suitable formulation for in vitro permeation testing of VHH using hydrogel-forming MAPs. Additionally, H1 had a VHH(HLE) recovery of  $100 \pm 3\%$  and was therefore considered suitable for in vitro testing of the half-life extended Nanobody format.

## 2.4. Short-Term Stability Testing on VHH and VHH(HLE) Solutions and Lyophilized Wafers

A 72-h stability test in different environmental conditions was performed to determine whether the formulation process of both Nanobody molecules into lyophilized wafers had an adverse effect on stability. To this end, the stability of the original VHH solution and VHH in F8 lyophilized wafers when exposed to different environmental conditions, namely refrigeration (4 °C), exposure to natural light at ambient temperature (20 °C), protection from natural light at ambient temperature and incubation at 37 °C, was directly compared over a 72 h study period. As highlighted in the SE-HPLC chromatograms shown in Figure 3a–e, the retention times of VHH-loaded lyophilized wafers remained unchanged (18.6 min) for all conditions after dilution in PBS over

a 72-h period. Additionally, no aggregate or degradant peaks were observed. Directly comparing F8 wafers with the original VHH solution in each condition (Figure 3f) revealed no statistically significant differences, except for the ambient light protected % recovery, where on average a 13% difference was observed. That said, this short-term study has shown that the wafer manufacturing process did not adversely affect VHH stability.

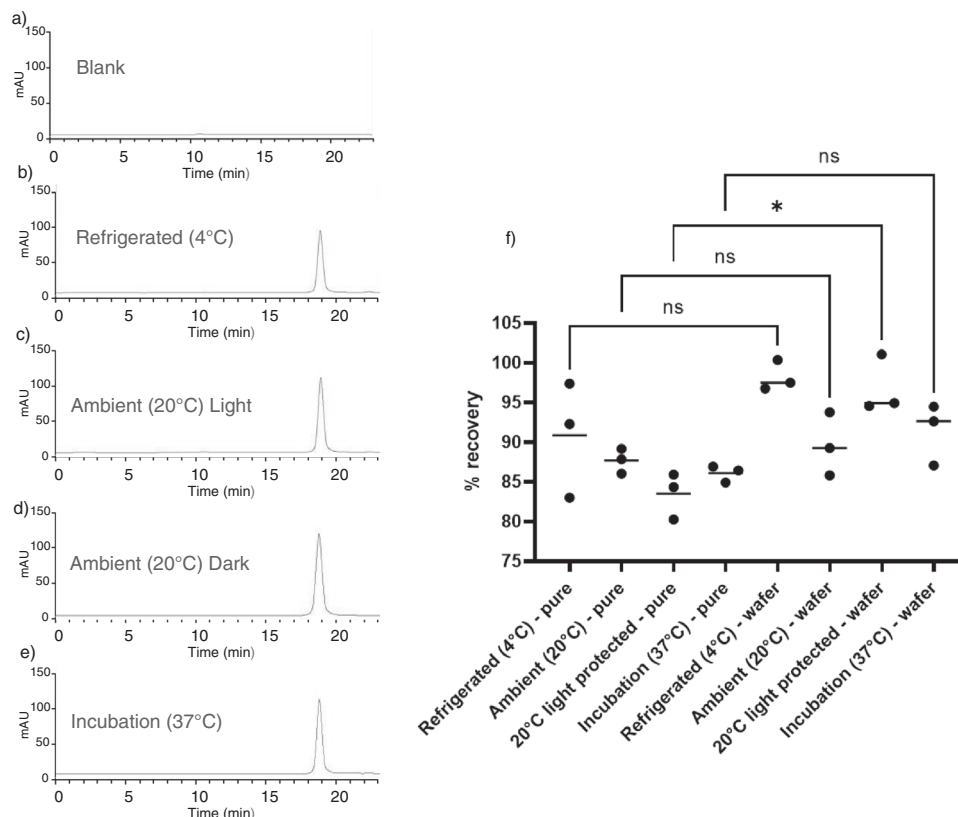
As was observed with VHH, the retention times of VHH(HLE) after 72 h for H1 lyophilized wafers subjected to four different conditions in PBS remained unchanged (19.3 min). The absence of additional peaks within each trace provides further evidence that the VHH(HLE) remains stable over the 72-h study period (Figure 4a–e). Directly comparing H1 wafers with the original VHH(HLE) solution in each condition (Figure 4f) revealed no statistically significant differences, showing that in a similar manner to VHH, the stability of VHH(HLE) was maintained during the wafer manufacturing process.

## 2.5. Sodium Dodecyl Sulfate-Polyacrylamide Gel Electrophoresis (SDS-PAGE) Analysis

To further analyze both VHH and VHH(HLE) stability following exposure to different environmental conditions over 72 h, SDS-PAGE was performed. Figure 5a displays a NuPAGE Bis-Tris 4–12% 1.5 mm gel for VHH stock solutions and lyophilized wafers, in which VHH was reconstituted in PBS. Lanes 1–4 represent VHH stock solution following exposure to different environmental conditions for 72 h. Lanes 5–8 represent VHH loaded into lyophilized wafers. Each band within lanes 1–8 corresponds to a MW of 45 kDa. The presence of a single band within these lanes aligns with the SE-HPLC data, showing that the VHH remains stable following exposure to different environmental conditions for 72 h. As shown in Figure 5b, similar results were obtained for VHH(HLE), proving that this construct also remains stable in different environmental conditions over the 72-h study period.

## 2.6. In Vitro Permeation of VHH and VHH(HLE) using Hydrogel-Forming MAPs

In vitro permeation of VHH and VHH(HLE) through dermatomed neonatal porcine skin was assessed using different



**Figure 3.** SE-HPLC traces for VHH-loaded F8 lyophilized wafers following exposure to four different environmental conditions at 72 h. a) Blank lyophilized wafer, b) refrigerated at 4 °C, c) exposed to natural light at ambient temperature (20 °C), d) protected from natural light at ambient temperature (20 °C), and e) incubated at 37 °C. f) Percentage recovery of VHH original solution and F8 lyophilized wafers following dilution in PBS (pH 7.4) for 72 h and exposure to four environmental conditions. Means  $\pm$  SD.  $n = 3$ . ns: not significant at the 5% significance level, \*:  $0.05 < p \leq 0.1$ .

hydrogel-forming MAP formulations, namely PVP/PVA composed of an aqueous blend of 15% w/w PVA, 10% PVP & 1.5% w/w citric acid, “super-swellable Gantrez S-97 composed of an aqueous blend of 20% w/w Gantrez S-97, 7.5% w/w PEG 10000 and 3% w/w  $\text{Na}_2\text{CO}_3$ , and ‘swellable’ Gantrez S-97 composed of aqueous blend of 20% w/w Gantrez S-97, 7.5% w/w PEG 10000. All formulations have been characterized previously and have displayed suitable mechanical strength for skin insertion.<sup>[9–15]</sup>

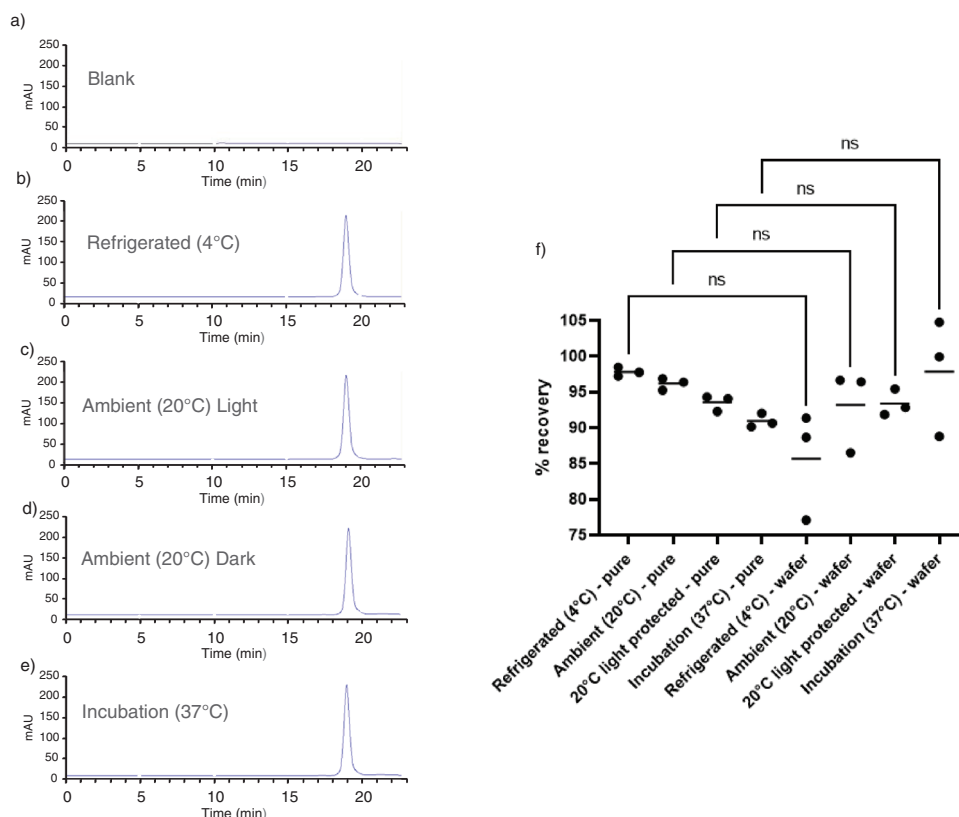
As shown in **Figure 6a**, PVP/PVA hydrogel-forming MAPs produced the greatest % VHH permeation, with  $46 \pm 6\%$ , equivalent to  $6.8 \pm 0.5$  mg, delivered after 24 h. Directly comparing this to “super-swellable” Gantrez S-97 MAPs, it is clear that this formulation resulted in a 5.25 fold decrease in permeation, with  $9 \pm 3\%$  ( $1.4 \pm 0.4$  mg) VHH delivered after 24 h. In addition, it was observed that “swellable” Gantrez S-97 MAPs delivered the lowest amount of VHH, equivalent to  $4 \pm 2\%$  ( $0.5 \pm 0.2$  mg). Interestingly, the “swellable” MAPs delivered a significantly lower amount of VHH than its “super-swellable” counterpart ( $p < 0.05$ ), illustrating that a greater degree of swelling does result in greater permeation across the skin using a Gantrez S-97-based formulation as previously thought. Nevertheless, the low amount of VHH delivered using the “super-swellable” MN suggests that the protein interacts with a component within the hydrogel formulation. This has been observed previously and is hypothesized to be a result of charge interactions between the carboxyl group on the

polymer and the positively charged proteins in the presence of PBS (pH 7.4).<sup>[9,10]</sup> As shown in these results, changing the MAP formulation to PVP/PVA has minimized such interactions, enabling greater amounts of drug to be delivered in vitro.

In vitro permeation of VHH(HLE) through dermatomed neonatal porcine skin was then assessed using both PVP/PVA & “super swellable” Gantrez S-97 hydrogel-forming MAP formulations (**Figure 6b**). As observed with VHH, PVP/PVA hydrogel-forming MAPs produced the greatest % VHH(HLE) permeation, with  $62 \pm 15\%$  ( $8.3 \pm 2.1$  mg) delivered after 24 h. Using a *t*-test and applying the Satterthwaite–Welch correction to acknowledge the variance differences between the two MAP formulations, it is evident that the “super-swellable” Gantrez S-97 MAPs delivered a significantly lower amount of VHH(HLE) ( $p = 0.0026$ ), with only  $11 \pm 0.2\%$  ( $1.6 \pm 0.04$  mg) delivered after 24 h. Again, this could be due to electrostatic interactions, as Gantrez S-97 has a higher MW and more electronegative oxygen atoms compared to PVA and PVP.

### 2.7. In Vivo Delivery of VHH, VHH(HLE), and BEV in Sprague–Dawley Rats

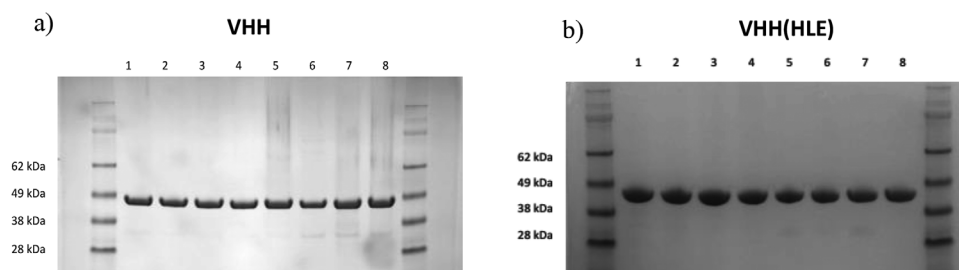
An in vivo delivery study of VHH and VHH(HLE) was conducted in female Sprague–Dawley rats aged 12 weeks to provide insights



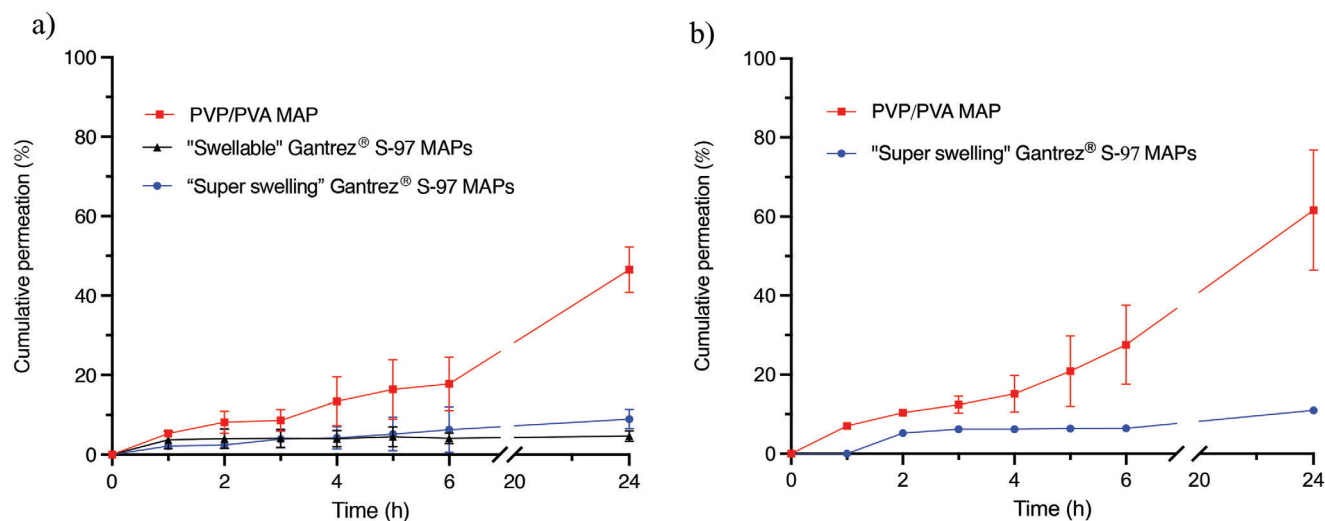
**Figure 4.** SE-HPLC traces for VHH(HLE) loaded lyophilized wafers following exposure to four different environmental conditions at 72 h. a) Blank lyophilized wafer, b) refrigerated at 4 °C, c) exposed to natural light at ambient temperature (20 °C), d) protected from natural light at ambient temperature (20 °C), e) incubated at 37 °C. f) Percentage recovery of VHH(HLE) original solution and H1 lyophilized wafers following dilution in PBS (pH 7.4) for 72 h and exposure to four environmental conditions. Means  $\pm$  SD.  $n = 3$ . ns: not significant at the 5% significance level.

on the predictivity of the in vitro model. The PVP/PVA hydrogel-forming MAP formulations were applied to the backs of shaved rats which were subjected to a hair removal procedure 24 h prior to MAP application. In both MAP cohorts, the lyophilized wafers had fully dissolved after 24 h, leaving no observable residue on the MAP or release lining film (Figure 7a). Following the removal of the hydrogel-forming MAPs, microchannels at the application site remained clearly visible (Figure 7b). In both cohorts, PVP/PVA MAPs had visibly swollen and were removed from the skin completely intact (Figure 7c,d). For the VHH, blood samples

were taken at defined intervals for 5 days. Due to the increased half-life of VHH(HLE), blood samples were taken over a 7-day period. In all cases, serum was extracted and stored at  $-80$  °C, undergoing one freeze-thaw cycle prior to PK analysis. For comparison with MAP delivery, a study in Female Sprague-Dawley rats was conducted via SC administration. VHH and VHH(HLE) were administered via a single SC injection at  $3 \text{ mg kg}^{-1}$ . Blood samples were collected at 1, 3, 6, 24, 32, 48, 72, 120, and 168 h and processed into serum, which was stored at  $-80$  °C. Samples underwent one freeze-thaw cycle prior to PK analysis.



**Figure 5.** SDS-PAGE analysis for a) VHH and b) VHH(HLE) stock solutions and lyophilized wafers following exposure to four different environmental conditions for 72 h. Lane 1: Lyophilized wafer at 20 °C (light); lane 2: Lyophilized wafer at 20 °C (dark); lane 3: Lyophilized wafer at 37 °C; lane 4: Lyophilized wafer at 4 °C; lane 5: Stock solution at 20 °C (light); lane 6: Stock solution at 20 °C (dark); lane 7: Stock solution at 37 °C; lane 8: Stock solution at 4 °C.



**Figure 6.** Line graph showing cumulative a) VHH and b) VHH(HLE) permeation (%) across dermatomed neonatal porcine skin over 24 h. Means  $\pm$  SD,  $n = 3$  for PVP/PVA based MAPs,  $n = 3$  for "swellable" Gantrez S-97 MAP, and  $n = 3$  for "super swellable" Gantrez S-97 MAPs.

Comparing the in vivo serum profiles for VHH (Figure 7e), the SC control displayed a 54-fold higher maximal VHH serum concentration ( $C_{\max}$ ) when compared to the MAP cohort. Notably, however, MAP delivery sustained the release of VHH over the 24-h application period. In contrast, a sharp decline in VHH serum concentration after 6 h was observed in the SC control, as expected for non-HLE Nanobody molecules. More specifically, during the 24-h time period, the observed concentration for the MAP cohort was greater than the concentration of the SC control, equivalent to  $19 \pm 9$  and  $1.1 \pm 0.4$  ng mL<sup>-1</sup> respectively (Table 2). Interestingly, the MAP and SC cohorts for VHH(HLE) displayed a similar trend, both achieving a  $T_{\max}$  at 24 h (Figure 7f). It is evident that the SC cohort displayed a higher  $C_{\max}$  and AUC compared to the MAP cohort (Table 2). However, given the steep increase in serum concentration during the application period (24 h), one could hypothesize that greater levels could be achieved if the MAP application had extended beyond the 24 h time point.

Directly comparing the serum profiles for VHH and VHH(HLE) delivered via PVP/PVA hydrogel-forming MAPs, much higher VHH(HLE) levels were achieved (Figure 8). More specifically, a 156-fold higher VHH(HLE)  $C_{\max}$  was determined despite identical loading doses.

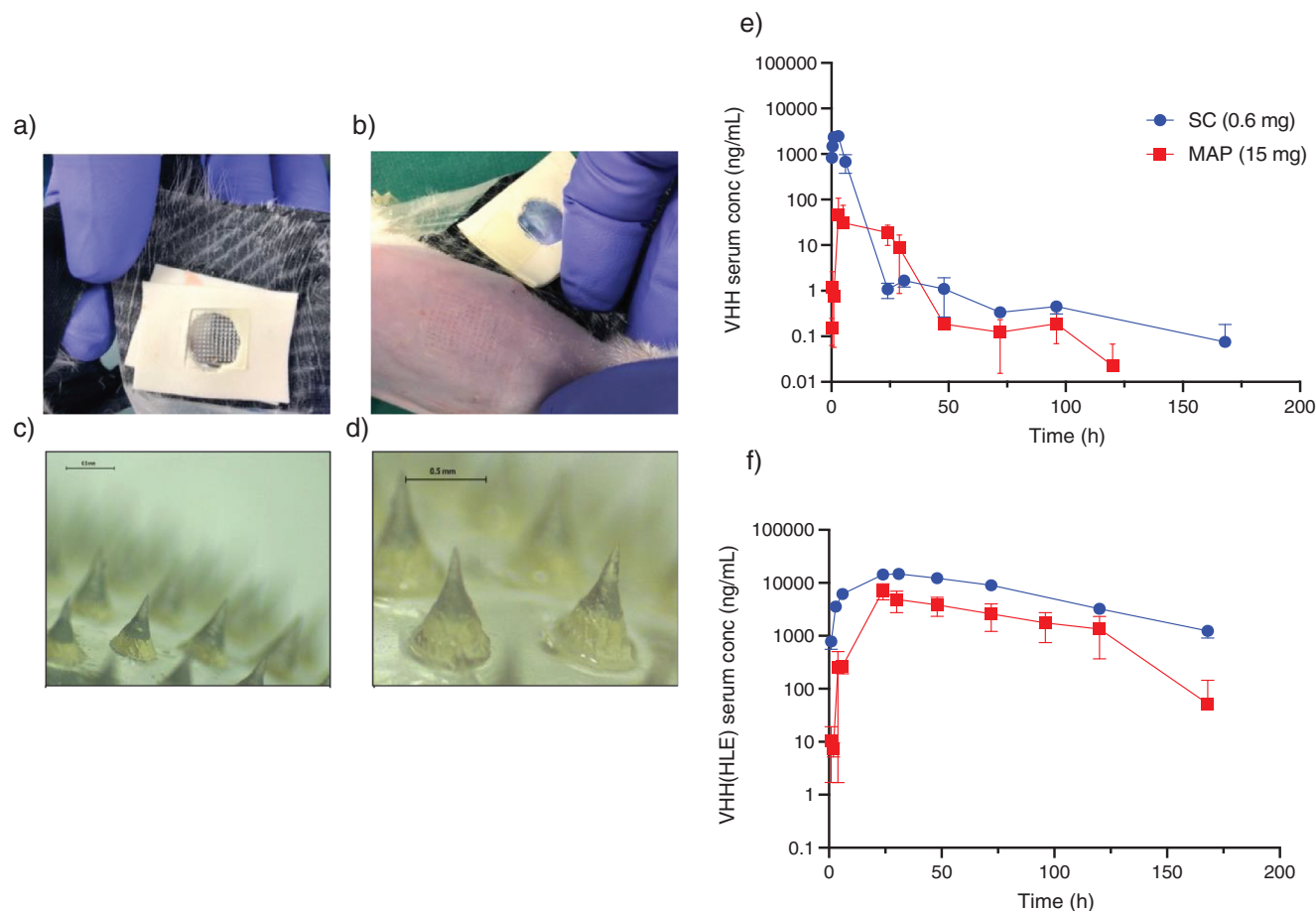
### 3. Discussion

Nanobody molecules are a novel class of proprietary therapeutic proteins based on single-domain antibody fragments of the heavy-chain only antibodies from species of Camelidae. Despite being a tenth of the size, they still maintain similar functional properties to conventional mAbs. Due to their small size and unique structure, Nanobody molecules are ideal building blocks for the next generation of novel biological drugs with multiple competitive advantages over the conventional mAb. For instance, they are readily expressed in bacteria and yeast in large quantities and show high thermal stability and solubility, making them easily scalable and cost-effective.<sup>[16,17]</sup> Furthermore, their modularity means that they can be formatted into multivalent constructs

to increase avidity or to increase serum half-life.<sup>[18]</sup> For this reason, there are currently more than 45 Nanobody molecules in development for the treatment of a wide range of diseases, including inflammation, hematology, respiratory disease, and immunoncology. Interestingly, pharmaceutical companies actively working in this area have been searching for needle-free administration of Nanobody molecules. Currently, the nasal,<sup>[19]</sup> oral,<sup>[20]</sup> and ocular<sup>[21]</sup> routes have been investigated. Transdermal delivery using hydrogel-forming MAPs could also offer a unique administration route for Nanobody molecules. Such MAPs have the potential to allow systemic delivery of therapeutic doses of Nanobody molecules without the need for a conventional needle and syringe injection, thereby taking delivery of these advanced new therapeutic agents out of the in-patient setting and into the hands of patients in their own homes.

In this study, eight different lyophilized wafer formulations containing VHH were initially prepared. Lyophilized wafers are hygroscopic and porous due to the removal of water. As a result, this creates a system where rapid hydration is favored when exposed to fluid and so dissolution is encouraged. Gelatin, mannitol, and sodium chloride were the main excipients used within each wafer formulation. Gelatin, a protein, provided structural strength and mannitol, a sugar alcohol, was used to increase the bulk content and to enhance the stability of the Nanobody molecule. This stabilizing effect is thought to occur through a hydrogen bonding interaction between the polyol and protein sidechains.<sup>[22]</sup> As the interaction between water and the Nanobody molecule is critical to maintaining conformational stability, this hydrogen-bonding interaction helps preserve the native structure during the lyophilization process.

To characterize each wafer and to determine the most suitable formulation for incorporation into hydrogel-forming MAPs, the homogeneous appearance, drug loading, mechanical integrity, dissolution time in PBS and % recovery were the key factors considered. Initially, 8.5 mg of VHH was loaded in lyophilized wafers F1-F6, however, altering the dimensions of the lyophilized wafer (F7 and F8) permitted a higher VHH loading (15 mg).



**Figure 7.** Digital images following in vivo delivery of VHH and VHH(HLE) using hydrogel-forming MAPs depicting; a) adhesive foam border with no visible residue on the MAP or release lining film and b) visible microchannels at the application site immediately after MAP removal. Light microscope images of MAPs from c) VHH(HLE) and d) VHH cohorts after 24 h. All MAPs were removed from the skin completely intact and displayed visible swellability. In vivo serum profiles for e) VHH in female Sprague-Dawley rats that received VHH (15 mg) using PVP/PVA hydrogel-forming MAPs (Means + S.D.,  $n = 2$  at 15 min, 30 min, 1 h, 3 h, and 5 h;  $n = 4$  at 24, 29, 48, 72, 96, and 120 h). and control cohort that received  $3 \text{ mg kg}^{-1}$  VHH via subcutaneous (SC) injection (Means + S.D.,  $n = 2$  at 15 min, 30 min, 1 h, 3 h, 5 h, 31 h, 48 h, 72 h, 96 h, 144 h, and 168 h;  $n = 4$  at 24 h). f) VHH(HLE) in female Sprague-Dawley rats for the treatment cohort that received VHH(HLE) (15 mg) using PVP/PVA hydrogel-forming MAPs (Means + S.D.,  $n = 2$  at 1, 2, 4, and 6 h;  $n = 4$  at 24, 29, 48, 72, 96, 120, and 168 h), SC injection cohort that received  $3 \text{ mg kg}^{-1}$  of VHH(HLE) (Means + S.D.,  $n = 2$  at 1, 3, 6, 31, 48, 72, 120, and 168 h;  $n = 4$  at 24 h).

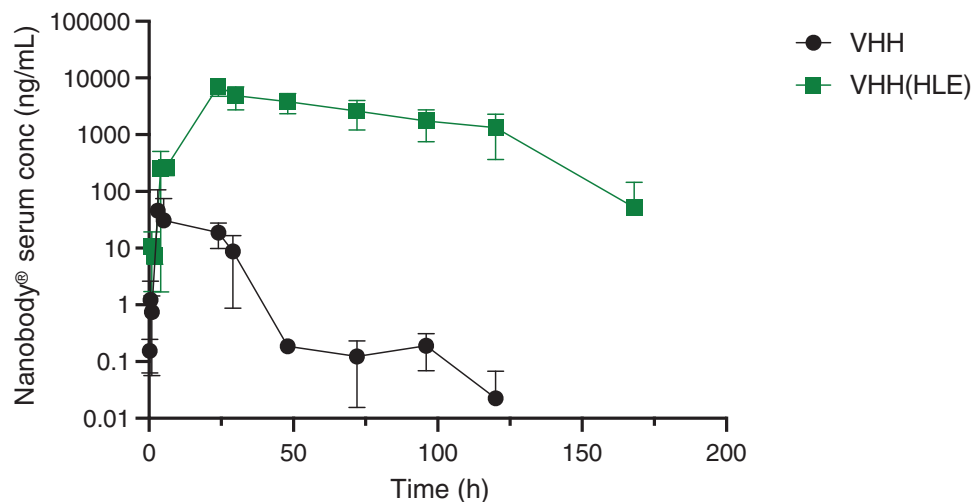
**Table 2.** Pharmacokinetic parameters of VHH and VHH(HLE) administered to female Sprague-Dawley rats using PVP/PVA MAPs and an SC injection. Means  $\pm$  SD,  $n = 4$ .

| Parameter                                | VHH           |                    | VHH(HLE)               |                           |
|--|---------------|--------------------|------------------------|---------------------------|
|  | MAP           | SC                 | MAP                    | SC                        |
| AUC [ $\text{ng}\cdot\text{h mL}^{-1}$ ] | $763 \pm 444$ | $16\,976 \pm 2844$ | $382\,620 \pm 54\,436$ | $1\,190\,981 \pm 40\,378$ |
| $T_{\text{max}}$ [h]                     | 3             | 3                  | 24                     | 24                        |
| $C_{\text{max}}$ [ $\text{ng mL}^{-1}$ ] | $62 \pm 46$   | $2481 \pm 355$     | $7182 \pm 2392$        | $14\,401 \pm 414$         |

Whilst it is assumed that this is not the maximum loading that can be achieved, this loading enabled high-dose delivery both in vitro and in vivo to be investigated. Examining each wafer (F1–F8), increasing the gelatin content resulted in a prolonged dissolution time. Nevertheless, increasing the gelatin concentration enhanced the wafer's structural integrity, permitting complete wafer removal from its cylindrical mold. Based on the key factors mentioned above, F8, fabricated from an aqueous blend

of 5.6% w/w gelatin, 20% w/w mannitol, 5.6% w/w NaCl, and 3% w/w VHH, was considered the most suitable wafer for further investigation. Whilst this wafer did have the slowest dissolution time, there must be a balance between dissolution time and structural integrity. This wafer remained structurally intact when subjected to a 30 N force, consistent with the force applied by human subjects after instruction. In addition, a dissolution time of  $\approx 5$  min was not considered extensive and was in line





**Figure 8.** Combined in vivo serum profiles for VHH(HLE) and VHH in female Sprague–Dawley rats for using PVP/PVA hydrogel-forming MAPs (Means  $\pm$  SD,  $n = 2$  at 1, 2, 4, and 6 h;  $n = 4$  at 24, 29, 48, 72, 96, 120, and 168 h for VHH(HLE) and Means  $\pm$  SD,  $n = 2$  at 15 min, 30 min, 1 h, 3 h, and 5 h;  $n = 4$  at 24, 29, 48, 72, 96, and 120 h for VHH).

with previous studies that utilized a lyophilized wafer alongside a hydrogel-forming MAP.<sup>[23,24]</sup> Based on the successful production of a VHH wafer, VHH(HLE) was incorporated into a lyophilized wafer containing the same composition as F8. As expected, this wafer (H1) remained homogeneous and structurally intact, passing the strength test and generating a high percentage recovery.

As an initial short-term stability assessment, both stock solutions and lyophilized formats of VHH and VHH(HLE) were examined over a 72-h period. Directly comparing the % recovery of VHH F8 wafers with the original solution, it is evident that the wafer manufacturing process did not adversely affect VHH stability. Importantly, this was also observed with VHH(HLE) H1 wafers. SDS-PAGE confirmed that the MW of both VHH and VHH(HLE) remained unchanged (45 kDa), with a single band representative of an absence of protein fragmentation and aggregation. While the exploration of accelerated storage conditions in accordance with ICH guidelines has yet to be investigated, this research has demonstrated the notable stability of Nanobody molecules, especially throughout the reservoir manufacturing process and exposure to diverse environmental conditions.

In vitro permeation of both VHH and VHH(HLE) through dermatomed (350  $\mu$ m) neonatal porcine skin was assessed using hydrogel-forming MAPs and Franz cell apparatus. The permeation of VHH was first investigated using both “swellable” and “super swellable” Gantrez S-97 hydrogel-forming MAPs. As expected, “super swellable” MAPs permitted greater skin permeation for both VHH and VHH(HLE) than its “swellable” counterpart which was in line with previous work, proving that the swellable capacity of the hydrogel plays a role in the permeation of high MW biomolecules.<sup>[10]</sup> That said, both formulations yielded low percentage permeation results. Further investigation using PVP/PVA MAPs resulted in a dramatic increase in percentage permeation, delivering over 50% of its payload. This was unexpected given the lower swellable capacity of this formulation when compared to the “super swellable” alternative. Rather, it was assumed that a more rigid structure would decrease the ability for the VHH to diffuse through the hydrogel and into the

receiver compartment, due to lesser space available for free movement of the VHH. An identical trend was also observed with the VHH(HLE), with “super swellable” MAPs producing a low percentage permeation after the 24-h study period. Again, PVP/PVA MAPs delivered over 50% of its payload, equivalent to milligram levels in vitro. Such levels have been achieved previously with the mAb, bevacizumab (Avastin), however, for the first time, milligram levels of two Nanobody molecules have been delivered across dermatomed skin, an important discovery for the future translation of this technology<sup>[24]</sup>

The in vivo study performed here is the first example of the successful delivery of heavy-chain only antibody domains using hydrogel-forming MAPs. In this study, the transdermal delivery of both VHH and VHH(HLE) was achieved using PVP/PVA hydrogel-forming MAPs. Similar to the in vitro permeation studies, hydrogel-forming MAPs in each rat cohort were removed after 24 h. Although the rats are highly mobile, upon removal of the Kinesiology tape, Tegaderm film, and Microfoam surgical tape, the MAPs remained inserted in the skin and each MAP had visibly swollen. Full dissolution of the API-loaded lyophilized wafers occurred in all cohorts. This proved that the swollen MAPs provided sufficient fluid to dissolve the lyophilized wafer, allowing the loaded Nanobody molecule to diffuse through the hydrated matrix and permeate into the viable skin layers via the microchannels produced by each individual needle.

As mentioned previously, both VHH and VHH(HLE) are model Nanobody molecules and exert no therapeutic effect. Nevertheless, given that for therapeutic indications, Nanobody doses of up to a few hundred mg are considered, the concentration used in the SC control group closely represents a relevant therapeutic dose. Therefore, the potential for MAPs to deliver therapeutic levels of a Nanobody was determined by directly comparing the permeation profiles to the SC injection. Comparing the serum profiles for VHH, it is evident that this construct is rapidly cleared from the bloodstream, as was expected based on the MW cutoff for glomerular filtration of 30–50 kDa,<sup>[25]</sup> and the absence of half-life extension via albumin binding. Despite the MAP dose

being 25 times higher than the SC injection, the AUC was  $\approx 20$ -fold lower than the SC cohort. One possible reason for this observation is the slower release profile associated with the MAP. When applied to the skin, the MAP must first absorb the interstitial fluid before dissolving the drug-loaded lyophilized wafer situated on top of the base plate. Therefore, the rapid clearance of VHH from the bloodstream and the slower release of VHH from the MAP when compared to an SC injection could be attributed to the lower drug levels within the serum. Despite the higher levels observed with the SC injection in the early time points, the serum concentration dropped sharply between 6–24 h, as expected of a non-half-life extended molecule. In contrast, the MAP cohort displayed sustained levels during this period, with the serum concentration much higher than the SC cohort. Following the removal of the MAP at 24 h, the serum concentrations dropped and remained comparable to the SC cohort for the remaining study period. This finding could have important benefits for compounds with  $C_{\max}$ -driven toxicity. Several biologics, including Nanobody molecules, have been investigated in cell-mediated immunotherapy, more specifically as T-cell engagers and natural killer cell engagers. Although in the early stages of development, these compounds are showing promising pre-clinical and clinical results.<sup>[26,27]</sup> Given that they are highly potent, they may indeed benefit from the low-dose, sustained-release profile observed with MAPs. In this case, painless administration using MAPs could certainly gain greater acceptance among patients.

With respect to the VHH(HLE), prolonged exposure and a considerably higher  $C_{\max}$  were observed when compared to the VHH. This is clearly attributed to albumin binding, increasing the half-life of a Nanobody molecule from hours to days. This enables the biomolecule to be released from the MAP over the 24-h application period without renal clearance having a significant impact on serum concentration levels, in contrast to VHH. Upon observation, it is apparent that the MAPs produced a similar serum profile to the SC route over the study period, however, the SC route did display a faster absorption rate within the initial 24 h. Interestingly, the MAP VHH(HLE) serum levels increased sharply between 6–24 h, before dropping following removal of the MAP. Therefore, it is conceivable that if the MAP was left on for longer than 24 h, the  $C_{\max}$  would be greater than what has been observed in this current study. As mentioned previously, this Nanobody molecule has no therapeutic effect, however, the SC dose used is in line with previous doses used for therapeutic Nanobody molecules.<sup>[28]</sup> Although there is a dose difference between the SC injection and MAP cohorts, this study has shown that similar levels of exposure can be achieved. Given that the hydrogel-forming MAP is not limited in terms of drug loading when compared to dissolving and coated MAP formulations, increasing the loading and/or the patch size would enable larger doses to be administered. Consequently, a balance must be struck between the efficiency of a traditional syringe and needle and the need for pain-free alternative methods of administration. With many different antibody-derived products on the market, pharmaceutical companies may be willing to pursue alternative methods of administration to gain an advantage over the competition. Given that Nanobody molecules are typically administered every 2–4 weeks over a prolonged period, the elimination of a hypodermic needle may be an attractive prospect for many suitable candidates. As a result, pharmaceutical companies

may be willing to invest in MAP technology due to its pain-free, patient-friendly method of administration.<sup>[29]</sup> This has the potential to generate larger revenue due to greater patient acceptance which could balance the increased cost associated with higher drug loadings. In conclusion, this study has demonstrated the potential for the transdermal delivery of Nanobody molecules using hydrogel-forming MAPs.

#### 4. Conclusion

Advances in antibody-based engineering have led to the development of therapeutic Nanobody molecules. These heavy chain only antibody domains derived from camelids possess several unique properties that have enabled alternatives to conventional needle and syringe administration to be explored. To date, transdermal delivery of these “next-generation” biotherapeutics has not been investigated. Here, the transdermal delivery of two Nanobody molecules, VHH and VHH(HLE), was examined using hydrogel-forming MAPs. Following in vivo administration, sustained levels of VHH over the 24-h application time were achieved using hydrogel-forming MAPs. Given the very short half-life of this construct, sustained serum levels could provide important benefits in the field of tumor imaging. Furthermore, the serum profile trend for VHH(HLE) was similar to that of the SC control. Therefore, the levels achieved in this study suggest that hydrogel-forming MAPs can deliver therapeutically relevant doses. This presents the opportunity to circumvent some of the drawbacks associated with traditional hypodermic needle and syringe administration. Therefore, this study has exemplified the use of MAP technology for the delivery of the next generation of biologics. With further optimization, hydrogel-forming MAP technology certainly has the potential to offer an attractive delivery route for Nanobody molecules.

#### 5. Experimental Section

**Materials:** VHH solution (59.3 mg mL<sup>-1</sup>) and VHH(HLE) solution (50.4 mg mL<sup>-1</sup>) were obtained from Sanofi Ghent, Technologiepark 21, 9052 Zwijnaarde, Belgium. Avastin concentrate solution for infusion 25 mg mL<sup>-1</sup> was purchased from Roche Welwyn Garden City, Hertfordshire, UK. Gantrez S-97, a co-polymer of methyl vinyl ether and maleic acid (PMVE/MA) was a gift from Ashland, Kidderminster, UK. Poly (ethylene glycol) (PEG) with MW = 10 000 Da, was purchased from Sigma-Aldrich, Steinheim, Germany. Sodium carbonate (Na<sub>2</sub>CO<sub>3</sub>) was purchased from BDH Laboratory Supplies, London, UK. Poly(vinylpyrrolidone) (PVP), MW 58 kDa, sold under the product brand name Plasdone K-29/32, was obtained from Ashland, Switzerland. Poly(vinyl acetate) (PVA), MW 85 000–124 000 Da was purchased from Sigma Aldrich, Steinheim, Germany. Citric acid was obtained from BHD Laboratory Supplies, Poole, UK. Cryogel SG3 was provided by PB Gelatins, Pontypridd, UK. Pearlitol 50C-Mannitol was supplied by Roquette, Lestrem, France. Sodium chloride (NaCl) was purchased from Sigma Aldrich, Steinheim, Germany. NuPAGE Bis-Tris 4–12% 1.5 mm 10 well gel, SeeBlue Plus 2 Pre-stained protein standard ladder, Coomassie blue R-250 dye and NuPAGE MES SDS Running Buffer were purchased from ThermoFisher Scientific, Rockford, USA. Recombinant human VEGF165 was purchased from Biologend San Diego, USA. Biotinylated VEGF165 was purchased from antibodies-online GmbH, Aachen, Germany. 1-Step Ultra TMB-ELISA substrate was purchased from ThermoFisher Scientific, Rockford, USA.

**Manufacture of VHH-Loaded Lyophilized Wafers:** To prepare VHH-loaded lyophilized wafers, gelatin, and sodium chloride was first dissolved

in deionized water, followed by the addition of mannitol. Once a homogeneous mixture was formed, the appropriate volume of VHH stock solution ( $59.3 \text{ mg mL}^{-1}$ ) was added. F1–F6 formulations were then cast into open-ended cylindrical molds with a diameter of 8 mm and depth of 5 mm, producing a final weight of 300 mg (Table 1). To facilitate higher drug loading (500 mg), F7 and F8 were added to open-ended cylindrical molds with a diameter of 12 mm and depth of 3 mm. Each formulation was subsequently frozen at  $-80^\circ\text{C}$  for 60 min, then lyophilized using a Virtis Advantage Benchtop Freeze Drier System, SP Scientific, Warminster PA, USA with a previously employed freeze-drying cycle.<sup>[9,23]</sup>

**Manufacture of VHH(HLE)-Loaded Lyophilized Wafers:** VHH(HLE)-loaded lyophilized wafers (H1) were prepared using the same composition as the F8 VHH wafers. To summarize, 5.6% w/w gelatin and 5.6% w/w sodium chloride were first dissolved in deionized water, followed by the addition of 20% w/w mannitol. Once a homogeneous mixture was formed, the appropriate volume of VHH(HLE) stock solution ( $50.4 \text{ mg mL}^{-1}$ ) was added. Each formulation was then cast into open-ended cylindrical molds with a diameter of 12 mm and depth of 3 mm. The formulation was subsequently lyophilized as detailed above.

**Strength Testing of VHH- and VHH(HLE)-Loaded Lyophilized Wafers:** To determine the strength of each wafer formulation, a TA.XT2 Texture Analyzer was used. Each wafer was placed on an aluminum block on the Texture Analyzer platform. A probe was lowered at a speed of  $1.19 \text{ mm s}^{-1}$  and a force of 30 N was applied to each wafer for 30 s. In this test, fracture or crumbling was considered a failed result.

**Dissolution Time and Recovery of VHH- and VHH(HLE)-Loaded Lyophilized Wafers:** To determine the dissolution time of each wafer formulation, 10 mL of PBS (pH 7.4) was added to glass vials, heated to  $37^\circ\text{C}$ , and stirred using a small magnetic bar ( $12 \times 6 \text{ mm}$ ) at 200 rpm. Lyophilized wafers were then added to PBS (pH 7.4) and the dissolution time was recorded from a visual inspection. VHH and VHH(HLE) recovery from each lyophilized wafer formulation was determined following wafer dissolution. This was achieved by sampling the dissolution medium, with samples filtered using  $0.45 \mu\text{m}$  VWR cellulose acetate syringe filters and quantified using SE-HPLC as detailed below.

**VHH and VHH(HLE) Stability Testing over 72 h:** Defined volumes of VHH ( $59.3 \text{ mg mL}^{-1}$ ) and VHH(HLE) ( $50.4 \text{ mg mL}^{-1}$ ) stock solutions were diluted in PBS (pH 7.4) in individual 15 mL falcon tubes ( $1.5 \text{ mg mL}^{-1}$ ) and subjected to four different storage conditions over 72 h. This included refrigeration ( $4^\circ\text{C}$ ), exposure to natural light at ambient temperature ( $20^\circ\text{C}$ ), protection from natural light at ambient temperature, and incubation at  $37^\circ\text{C}$ . Aluminum foil was used to provide protection from natural light. Aliquots (1 mL) were removed from three replicates at 24, 48, and 72 h, filtered using  $0.45 \mu\text{m}$  VWR cellulose acetate syringe filters, and analyzed using SE-HPLC. To determine VHH stability within F8 lyophilized wafers, VHH-loaded wafers were added to PBS in separate 15 mL falcon tubes to achieve a concentration of  $1.5 \text{ mg mL}^{-1}$  and subjected to the same storage conditions as mentioned previously. Similar conditions were used for the H1 VHH(HLE)-loaded lyophilized wafer. As before, 1 mL aliquots were removed from three replicates at 24, 48, and 72 h, filtered using  $0.45 \mu\text{m}$  VWR cellulose acetate syringe filters, and analyzed using SE-HPLC.

**Sodium Dodecyl Sulfate–Polyacrylamide Gel Electrophoresis (SDS-PAGE) Analysis:** VHH and VHH(HLE) samples exposed to the four different environmental conditions mentioned previously for 72 h were analyzed for stability by running down an SDS-PAGE gel followed by Coomassie blue staining. To begin, 50  $\mu\text{L}$  aliquots of each VHH or VHH(HLE) sample ( $\approx 15 \mu\text{g}$ ) were added to 10  $\mu\text{L}$  of  $5 \times$  Laemmli sample buffer (4 mL 1.5 M Tris-HCl pH 6.8, 10 mL glycerol, 5 mL  $\beta$ -mercaptoethanol, 2 g SDS, 1 mL 1% bromophenol blue) and exposed to  $100^\circ\text{C}$  for 10 min. Once the samples had cooled to room temperature, 30  $\mu\text{L}$  of each sample was loaded onto a NuPAGE Bis-Tris 4–12% 1.5 mm 10 well gel, in addition to a See-Blue Plus 2 Pre-stained protein standard ladder. Using NuPAGE MES SDS Running Buffer, the gel was run at a constant 200 V for 40 min. A staining solution containing Coomassie blue R-250, acetic acid, and ethanol was then added to the gel for 1 h. Following the removal of the staining solution, a destain solution containing methanol, acetic acid, and deionized water was added. This was removed after 1 h, replaced with fresh destain

solution, and left overnight. The gel was then washed with deionized water and imaged using a Syngene G:Box Chemi XRQ with GeneSys software.

**In Vitro Permeation of VHH and VHH(HLE) using Hydrogel-Forming MAPs:** Permeation studies for VHH and VHH(HLE) were carried out using Franz cell apparatus, with dermatomed neonatal porcine skin ( $350 \mu\text{m}$ , excised from stillborn piglets) as the test membrane. Three different  $11 \times 11$  hydrogel-forming MAP formulations were tested, namely PVP/PVA,<sup>[9,13]</sup> “swellable” Gantrez S-97,<sup>[30]</sup> and “super swellable” Gantrez S-97<sup>[12]</sup> (i.e., with the addition of  $\text{Na}_2\text{CO}_3$  to the formulation). Each MAP was composed of 121 conical needles,  $600 \mu\text{m}$  in height, interspacing  $300 \mu\text{m}$ , and base width  $300 \mu\text{m}$ . Each MAP type was inserted into the skin using manual pressure for 30 s, supported by a sheet of folded aluminum foil. A lyophilized wafer loaded with VHH or VHH(HLE) was then placed onto the upper surface of the array. A metal weight (13 g) was balanced on the lyophilized reservoir to ensure the MAPs remained inserted over the course of the 24-h experimental test period. Steel clamps secured the cell, and Parafilm M was used to cover the donor chamber to reduce water loss through evaporation. Regular samples were taken throughout the experimental time (24 h) and replaced with PBS preheated to  $37^\circ\text{C}$ .

**SE-HPLC for the Quantification of VHH and VHH(HLE) In Vitro:** SE-HPLC was used for the detection and quantification of VHH and VHH(HLE) from in vitro samples diluted in PBS (pH 7.4). In summary, analysis was carried out on an Agilent 1200 series system. The column used for separation was a Bio-Sep-SE-S 3000 column ( $5 \mu\text{m}$  particle size,  $290 \text{ \AA}$  pore size, and  $300 \text{ mm}$  length), maintained at  $20^\circ\text{C}$ . The optimized mobile phase was composed of 10 mM phosphate buffer, 150 mM L-Arginine HCl, 10% 1-propanolol, and 0.02% sodium azide (pH 7.4) at a flow rate of  $0.5 \text{ mL min}^{-1}$ . This was vacuum filtered using a  $0.22 \mu\text{m}$  filter prior to use. The injection volume was 10  $\mu\text{L}$ , with a sample run time of 30 min for VHH and 25 min for VHH(HLE). UV detection for both compounds was carried out at 280 nm. The limits of detection (LoD) and quantification (LoQ) for VHH and VHH(HLE) including the equation of regression line and linearity are further detailed in Table 3.

**In Vivo Subcutaneous Administration of VHH and VHH(HLE) in Sprague–Dawley Rats:** Female Sprague–Dawley rats (Charles River Laboratories, Sulzfeld, Germany), 12 weeks of age were acclimatized to laboratory conditions for a 7-day period prior to the commencement of the study. On the morning of dosing, the required number of aliquots of the test item stock solutions were thawed at  $+25^\circ\text{C}$  using a water bath and swirled gently for 5–10 min. Stock solutions were diluted in the appropriate volume of commercial and sterile D-PBS under laminar flow. VHH solution ( $1.5 \text{ mg mL}^{-1}$ ) was administered to the appropriate animals ( $n = 6$  per compound) via a single SC (neck, bolus) injection at  $3 \text{ mg kg}^{-1}$  on day 0.

Blood was collected at different time points (1, 3, 6, 24, 32, 48, 72, 120, and 168 h). Blood was sampled with a composite profile, with alternating blood collection from 1<sup>st</sup>–2<sup>nd</sup> and 3<sup>rd</sup>–4<sup>th</sup> animals of the group. The animals were restrained during blood sampling for intermediate sampling. Blood (200  $\mu\text{L}$  per sample) from the saphenous vein was collected in labeled 200  $\mu\text{L}$  non-anticoagulated microtubes. Immediately following collection, blood samples were slowly homogenized and stored at room temperature. For terminal sampling, blood was collected via axillary cut-down following isoflurane inhalation anesthesia. Blood samples were collected into labeled 8 mL non-anticoagulated poly(propylene) tubes. In vivo experiments were conducted according to the policy of the Federation of European Laboratory Animal Science Associations and the European Convention for the protection of vertebrate animals used for experimental and other scientific purposes, with the implementation of the principles of the 3Rs (replacement, reduction, and refinement). The study was conducted in compliance with the Sanofi institutional animal care policy. Serum was prepared by placing 200  $\mu\text{L}$  of whole blood on the benchtop at room temperature for 30 min undisturbed to facilitate clotting. The samples were then centrifuged at  $4^\circ\text{C}$  for 10 min at 1500 g, and the supernatant (serum) apportioned into 50  $\mu\text{L}$  aliquots in clean non-anticoagulated poly(propylene) 0.5 mL tubes and stored at  $-80^\circ\text{C}$ . Each sample was subject to one freeze-thaw cycle prior to analysis.

**In Vivo MAP Administration of VHH and VHH(HLE) in Sprague–Dawley Rats:** Female Sprague–Dawley rats (Charles River Laboratories, Harlow, UK), 12 weeks of age were acclimatized to laboratory conditions for a 7-

**Table 3.** Calibration parameters for VHH and VHH(HLE) SE-HPLC detection, as represented by the equation of the regression line, coefficient of determination ( $R^2$ ), LoD, and LoQ.

| Analyte  | Equation of regression line | Linearity [ $R^2$ ] | LoD [mg mL <sup>-1</sup> ] | LoQ [mg mL <sup>-1</sup> ] |
|----------|-----------------------------|---------------------|----------------------------|----------------------------|
| VHH      | $y = 2724.5x - 161.96$      | 1                   | 0.06                       | 0.17                       |
| VHH(HLE) | $y = 2312x - 56.757$        | 1                   | 0.03                       | 0.1                        |

day period prior to the commencement of the study. After this period, a PVP/PVA hydrogel-forming MAP in addition to a lyophilized wafer loaded with VHH (15 mg) or VHH(HLE) (15 mg) was applied to the back of each rat. Prior to MAP application, animals were anesthetized using isoflurane (2% to 4% in oxygen). The backs of the rats were then clipped using clippers before hair removal cream was applied for 10 min to remove all remaining hairs in the MAP application area. Each rat was then left to recover for 24 h. PVP/PVA MAPs were then applied to a pinched section of skin on the back of each rat. An aliquot (10  $\mu$ L) of water was spotted on the back of the MAP base plate and the designated lyophilized wafer housed within an adhesive foam border was placed on top. The Tegaderm film was then placed over the MAPs and Kinesiology tape was gently wrapped around the back and abdomen of the rat to ensure the patches remained firmly in place for 24 h.

Blood samples (200  $\mu$ L) were collected into 1.5 mL non-anticoagulated poly(propylene) tubes via lateral tail vein bleed at predefined time points. Prior to sampling, each rat was individually placed into a heat box at < 39 °C for a maximum of 10 min. All rats were monitored following each tail vein bleed and assessed for signs of distress or adverse reaction. In each case, no adverse effects were reported. Importantly, all in vivo experiments were conducted according to the policy of the Federation of European Laboratory Animal Science Associations and the European Convention for the protection of vertebrate animals used for experimental and other scientific purposes, with the implementation of the principles of the 3Rs (replacement, reduction, and refinement). The study was conducted in compliance with the Sanofi institutional animal care policy.

Serum was prepared by placing 200  $\mu$ L of whole blood in an incubator at 37 °C for 40 min undisturbed to facilitate clotting. The samples were then centrifuged at 4 °C for 10 min at 2000 g, and the supernatant (serum) was apportioned into 50  $\mu$ L aliquots in clean non-heparinized poly(propylene) 0.5 mL tubes and stored at -80 °C. Each sample was subject to one freeze-thaw cycle prior to analysis.

**PK Assay for the Quantification of VHH and VHH(HLE) In Vivo:** The PK assay used for the detection and quantification of VHH and VHH(HLE) from in vivo Sprague–Dawley rat serum matrices was performed on the Meso Scale Discovery (MSD) platform. In summary, 150  $\mu$ L of Superblock T20 was first dispensed into each well of a streptavidin-coated MSD GOLD 96-well SMALLSPOT plate and incubated at room temperature (RT) for 1 h. To wash the plate, each well was filled with PBS/0.05% Tween 20 (300  $\mu$ L) and repeated three times. Wash steps were performed using an automated plate washer (Biotek 405 TS). Following this, 1  $\mu$ g mL<sup>-1</sup> of a biotinylated capture antibody diluted in PBS/1% Casein + 0.05% Tween 20 was added to each well (50  $\mu$ L) and incubated at RT for 1 h. The wash cycle was then repeated a further three times. Calibration standards (50  $\mu$ L) for both VHH and VHH(HLE), prepared in the range of 1110341.3 to 6.2 pg mL<sup>-1</sup> in rat serum, were added in duplicate to their respective wells. Calibrators, QC samples, and study samples were diluted 1:20 in the assay. The dynamic range was 70 pg mL<sup>-1</sup> (LLOQ) to 331 445 pg mL<sup>-1</sup> (ULOQ). After a 3 h incubation period at room temperature (RT), a further wash cycle was performed. A 0.5  $\mu$ g mL<sup>-1</sup> sulfo-tagged detection antibody, diluted in PBS/1% Casein + 0.05% Tween 20, was added to each well (50  $\mu$ L), with the plate covered from light and incubated at RT for 1 h. A final wash step was then performed before the addition of MSD GOLD read buffer A (150  $\mu$ L per well). The plate was then read within 10 min after adding the read buffer using an MSD Sector Imager Quickplex SQ 120.

**Pharmacokinetic (PK) Analysis:** Basic PK parameters were assessed following the application of a single hydrogel-forming MAP. The maximum serum concentration ( $C_{max}$ ) of VHH and VHH(HLE) and the time of maximum concentration ( $T_{max}$ ), were determined by inspection of the raw data.

The area under the curve (AUC), in this case, the serum concentration–time curve from time zero ( $t = 0$ ) to the last experimental time point ( $t = 120$  h for VHH and  $t = 168$  h for VHH[HLE]) for each rat cohort was calculated using the linear-log trapezoidal method. In the logarithmic trapezoidal method, the AUC between two-time intervals ( $t_2 - t_1$ ) and the natural log of their corresponding concentrations ( $\ln(C_1) - \ln(C_2)$ ) was calculated using Equation (1).

$$AUC_{t_1-t_2} = \frac{(C_1 - C_2)}{\ln(C_1) - \ln(C_2)} (t_2 - t_1) \quad (1)$$

**Statistical Analysis:** Statistical analysis was performed using SAS v9.4 (SAS Institute Inc., Cary, NC, USA) in GraphPad Prism v9.5.0 (GraphPad Software Inc., San Diego, California) on the Windows 10 platform. For the comparison of the VHH and VHH(HLE) original solutions and lyophilized wafers at 72 h for the four environmental conditions, Welch ANOVAs with Dunnett's T3 multiple comparisons tests were implemented. Cumulative permeation comparisons of MAP formulations at the 24-h time point were assessed by one-way analysis of variance (ANOVA) (for VHH) and Welch *t*-test (for VHH(HLE)) upon log-transformation of the cumulation permeation percentage, followed by step-down Bonferroni multiple testing correction. Effect sizes were back-transformed to yield fold changes.  $p < 0.05$  denoted statistical significance. All data was performed in triplicate unless otherwise stated.

## Acknowledgements

This work was supported by a grant from Ablynx NV, 9052 Zwijnaarde, Belgium. Aaron R.J. Hutton was funded by the Department for the Economy (N. Ireland) studentship. The authors acknowledge Abdullah Kandira and Tobias Paehler for support with the in vivo subcutaneous injection PK study, Els Pattyn for statistics support, and Gustavo Rivera for critical review of the manuscript.

## Conflict of Interest

Ryan Donnelly is an inventor of patents that have been licenced to companies developing microneedle-based products and is a paid advisor to companies developing microneedle-based products. The resulting potential conflict of interest has been disclosed and is managed by Queen's University Belfast. Tom Van Bogaert, Peter Casteels, Ortwijn Van de Vyver, Christelle Nonne, Veronique De Brabandere are employees of Sanofi and may hold shares and/or stock options in the company.

## Data Availability Statement

The data that support the findings of this study are available from the corresponding author upon reasonable request.

## Keywords

biotherapeutics, hydrogel-forming, microarray patch, transdermal

Received: January 24, 2024

Revised: March 7, 2024

Published online:

- [1] C. Hamers-Casterman, T. Atarhouch, S. Muyldermans, G. Robinson, C. Hammers, E. Bajyana Songa, N. Bendahman, R. Hammers, *Nature* **1993**, 363, 446.
- [2] E. A. Padlan, *Mol. Immunol.* **1994**, 31, 169.
- [3] Z. Zhou, T. C. Nguyen, P. Guchhait, J. F. Dong, *Semin. Thromb. Hemostasis* **2010**, 36, 71.
- [4] M. Scully, S. R. Cataland, F. Peyvandi, P. Coppo, P. Knöbl, J. A. Kremer Hovinga, A. Metjian, J. de la Rubia, K. Pavenski, F. Callewaert, D. Biswas, H. De Winter, R. K. Zeldin, *N. Engl. J. Med.* **2019**, 380, 335.
- [5] C. Palomo, V. Mas, L. Detalle, E. Depla, O. Cano, M. Vázquez, C. Stortelers, J. A. Melero, *Antimicrob. Agents Chemother.* **2016**, 60, 6498.
- [6] A. Amcheslavsky, A. L. Wallace, M. Ejemel, Q. Li, C. T. McMahon, M. Stoppato, S. Giuntini, Z. A. Schiller, J. R. Pondish, J. R. Toomey, R. M. Schneider, J. Meisinger, R. Heukers, A. C. Kruse, E. M. Barry, B. G. Pierce, M. S. Klempner, L. A. Cavacini, Y. Wang, *Sci. Rep.* **2021**, 11, 2751.
- [7] R. Al-kasasbeh, A. J. Brady, A. J. Courtenay, E. Larrañeta, M. T. C. McCrudden, D. O. Kane, S. Liggett, R. F. Donnelly, *Drug Delivery Transl. Res.* **2020**, 10, 690
- [8] S. Hoefman, I. Ottevaere, J. Baumeister, M. Sargentini-Maier, *Antibodies* **2015**, 4, 141.
- [9] A. R. J. Hutton, O. Ubah, C. Barelle, R. F. Donnelly, *J. Pharm. Sci.* **2022**, 111, 3362.
- [10] A. R. J. Hutton, M. T. C. McCrudden, E. Larrañeta, R. F. Donnelly, *J. Mater. Chem. B* **2020**, 8, 4202.
- [11] R. F. Donnelly, T. R. R. Singh, D. I. J. Morrow, D. A. Woolfson, *Microneedle-Mediated Transdermal and Intradermal Drug Delivery*, 1st ed., John Wiley & Sons, Ltd, Sussex, **2012**.
- [12] R. F. Donnelly, M. T. C. McCrudden, A. Zaid Alkilani, E. Larrañeta, E. McAlister, A. J. Courtenay, M.-C. Kearney, T. R. R. Singh, H. O. McCarthy, V. L. Kett, E. Caffarel-Salvador, S. Al-Zahrani, D. A. Woolfson, *PLoS One* **2014**, 9, e111547.
- [13] I. A. Tekko, G. Chen, J. Domínguez-Robles, R. R. S. Thakur, I. M. N. Hamdan, L. Vora, E. Larrañeta, J. C. McElnay, H. O. McCarthy, M. Rooney, R. F. Donnelly, *Int. J. Pharm.* **2020**, 586, 119580.
- [14] A. J. Courtenay, E. McAlister, M. T. C. McCrudden, L. Vora, L. Steiner, G. Levin, E. Levy-Nissenbaum, N. Shterman, M. C. Kearney, H. O. McCarthy, R. F. Donnelly, *J. Controlled Release* **2020**, 322, 177.
- [15] Y. A. Naser, I. A. Tekko, L. K. Vora, K. Peng, Q. K. Anjani, B. Greer, C. Elliott, H. O. McCarthy, R. F. Donnelly, *J. Controlled Release* **2023**, 356, 416.
- [16] L. Hanke, L. Vidakovics Perez, D. J. Sheward, H. Das, T. Schulte, A. Moliner-Morro, M. Corcoran, A. Achour, G. B. Karlsson Hedestam, B. M. Hällberg, B. Murrell, G. M. McInerney, *Nat. Commun.* **2020**, 11, 4420.
- [17] M. De Groeve, B. Laukens, P. Schotte, *Microb. Cell Fact.* **2023**, 22, 135.
- [18] P. Bannas, J. Hambach, F. Koch-Nolte, *Front. Immunol.* **2017**, 8, 1603.
- [19] L. Detalle, T. Stohr, C. Palomo, P. A. Piedra, B. E. Gilbert, V. Mas, A. Millar, U. F. Power, C. Stortelers, K. Allosery, J. A. Melero, E. Depla, *Antimicrob. Agents Chemother.* **2016**, 60, 6.
- [20] W. Wu, L. Shi, Y. Duan, S. Xu, L. Shen, T. Zhu, L. Hou, X. Meng, B. Liu, *Biomaterials* **2021**, 274, 120870.
- [21] H. Fuchs, L.-Z. Chen, S. Low, H. Yu, *Exp. Eye Res.* **2021**, 205, 108486.
- [22] M. Johnson, *Mater. Methods* **2012**, 2, 120.
- [23] E. M. Migdadi, A. J. Courtenay, I. A. Tekko, M. T. C. McCrudden, M.-C. Kearney, E. McAlister, H. O. McCarthy, R. F. Donnelly, *J. Controlled Release* **2018**, 285, 142.
- [24] A. J. Courtenay, M. T. C. McCrudden, K. J. McAvoy, H. O. McCarthy, R. F. Donnelly, *Mol. Pharm.* **2018**, 15, 3545.
- [25] A. Ruggiero, C. H. Villa, E. Bander, D. A. Rey, M. Bergkvist, C. A. Batt, K. Manova-Todorova, W. M. Deen, D. A. Scheinberg, M. R. McDevitt, *Proc. Natl. Acad. Sci. U. S. A.* **2010**, 107, 12369.
- [26] A. Maali, M. Gholizadeh, S. Feghhi-Najafabadi, A. Noei, S. S. Seyed-Motahari, S. Mansoori, Z. Sharifzadeh, *Front. Immunol.* **2023**, 14, 1012841.
- [27] J. Hambach, A. M. Mann, P. Bannas, F. Koch-Nolte, *Front. Immunol.* **2022**, 13, 1005800.
- [28] M. Van Roy, C. Ververken, E. Beirnaert, S. Hoefman, J. Kolkman, M. Vierboom, E. Breedveld, B. 't Hart, S. Poelmans, L. Bontinck, A. Hemeryck, S. Jacobs, J. Baumeister, H. Ulrichs, *Arthritis Res. Ther.* **2015**, 17, 135.
- [29] S. Kaushik, a H. Hord, D. D. Denson, D. V. McAllister, S. Smitra, M. G. Allen, M. R. Prausnitz, *Anesth. Analg.* **2001**, 92, 502.
- [30] R. F. Donnelly, T. R. R. Singh, M. J. Garland, K. Migalska, R. Majithiya, C. M. McCrudden, P. L. Kole, T. M. T. Mahmood, H. O. McCarthy, A. D. Woolfson, *Adv. Funct. Mater.* **2012**, 22, 4879.